Full Paper submitted to:
Magnetic Resonance in Medicine → Computer Processing and Modeling

Global Sensitivity Analysis of Skeletal Muscle dMRI Metrics: Effects of Microstructural and PGSE Pulse Parameters

Noel M. Naughton[1] and **John G. Georgiadis**[1,2]

[1]Department of Mechanical Science & Engineering, University of Illinois at Urbana-Champaign, Urbana IL, USA;

[2]Department of Biomedical Engineering, Illinois Institute of Technology, Chicago IL, USA

Email:

NM Naughton – nnaught2@illinois.edu

JG Georgiadis –jgeorgia@iit.edu

Abstract

Purpose: Estimating microstructural parameters of skeletal muscle from diffusion MRI (dMRI) signal requires first understanding the relative importance of these parameters, as well as the dMRI sequence parameters, on the signal. The purpose of this study is to determine the sensitivity of the dMRI signal and related metrics to variations in muscle microstructure and dMRI pulse parameters, as well as assess the effect of noise on these sensitivity relationships.

Methods: Using a simplified geometric model of skeletal muscle, numerical solutions of the Bloch-Torrey equation were used to calculate global sensitivity indices for seven microstructural and two PGSE pulse parameters. The effect of noise was considered by adding synthetic noise at two levels (SNR = 50 and 100). The microstructural parameters examined were muscle cell diameter, cell volume fraction, membrane permeability, intra- and extracellular diffusion coefficients, and intra- and extracellular T_2 times.

Results: The computed sensitivity indices show that the effect of noise is important but averaging the signal over multiple realizations mitigates the effect. Among the examined parameters, the two diffusion coefficients have the largest effect, and the myocyte diameter is more influential than permeability in the transverse direction. Finally, the dMRI metrics are sensitive to extracellular parameters, suggesting that extracellular structural information can be extracted by solving the corresponding inverse problems.

Conclusion: With the identification of key microstructural features that affect dMRI measurements, these sensitivity results can help interpret dMRI measurements of skeletal muscle in light of the underlying microstructure and further develop parsimonious dMRI models of skeletal muscle.

Keywords: sensitivity analysis; Bloch-Torrey equation; lattice Boltzmann method; diffusion MRI; skeletal muscle

Word count: 4987/5000

Figures: 3/10

1 Introduction

Changes in skeletal muscle pathology are associated with changes in the tissue microstructure. Examples include increased fibrosis due to injury and muscular dystrophy [1], changes in fiber type and cross sectional area due to aging [2, 3], and increased membrane permeability due to sarcolemma damage from muscular dystrophy [4, 5]. Measuring these microstructural changes is of interest in better understanding these pathologies, however, such measurements are difficult. Investigating the behavior of muscle via extraction of muscle for histological assay is highly invasive and time consuming. The extraction process may also change the morphological features being examined [6]. Diffusion MRI (dMRI) is a promising method that is sensitive to changes in the underlying microstructure. Much work has been done in white matter to elucidate the relationship between the dMRI signal and the underlying axonal structure [7]. dMRI can be similarly applied in skeletal muscle, however, the relationship is less understood due in large part to difficulties in signal acquisition caused by the relatively short T_2 of skeletal muscle [8]. Additionally, the larger cell size and dense packing of muscle's makes some popular white matter models inappropriate for use in skeletal muscle [9].

Skeletal muscle consists of an ordered, hierarchical organization of muscle cells surrounded by an extracellular collagen matrix and bundled together into fascicles, which are themselves bundled to form the whole muscle. This well ordered structure allows representation of an imaging voxel by a simplified repeating elementary volume (REV), which can be parameterized to allow systematic investigation of how changes in the REV effect the dMRI signal. Others have examined structural variations using Monte Carlo simulations [10–12], however, a comprehensive analysis of how microstructural and pulse parameters affect the dMRI signal has not been completed. Further, there are conflicting results regarding the relative influence of membrane permeability and fiber diameter [10, 11]. Previous studies have examined either a limited number of parameter combinations or used a limited number of microstructural and pulse parameters in their model. As such, it is uncertain whether the sensitivity relationships reported represent the global influence of a parameter, or if they reflect local interactions dependent on other parameters. To address this uncertainty, we identify seven microstructural parameters that we believe comprehensively parameterize muscle microstructure as well as two pulse parameters. We examine these nine parameters to understand their influence on dMRI signal. Using a lattice Boltzmann method solution of the Bloch-Torrey equation applied to an REV of muscle, we perform a global sensitivity analysis of the influence microstructural and dMRI pulse parameters have on dMRI metrics such as fractional anisotropy and mean diffusivity. This analysis comprehensively samples the possible combinations of parameters to determine which parameters have the largest effect on measured

dMRI metrics. The results will assist in proper parameterization of dMRI models by identifying which microstructural parameters are essential to modeling dMRI signal variation and which can safely be ignored or help constant.

The purpose of this paper is to determine the sensitivity of dMRI measurements to variations in microstructural and dMRI pulse parameters as well as assess the effect of dMRI signal noise on these sensitivity relationships. While similar questions have been asked previously [10–12], here the entire input space of both microstructural and pulse parameters is examined in order to identify key sensitivity relationships. This includes analysis of compartment specific diffusion coefficients as well as a broad range of sarcolemma permeability, which has not previously been done. These sensitivity results will help interpret dMRI measurements in terms of the underlying microstructural parameters. They will also inform further model development by identifying insensitive microstructural parameters, allowing for a reduction in the number of requisite independent model parameters.

2 Methods

dMRI Representation

The time evolution of dMRI signal is described by the Bloch-Torrey equation [13]

$$\frac{\partial \boldsymbol{M}(\boldsymbol{x},t)}{\partial t} = -i(\gamma \boldsymbol{G}(t)\cdot\boldsymbol{x})\boldsymbol{M}(\boldsymbol{x},t) - \frac{\boldsymbol{M}(\boldsymbol{x},t)}{T_2} - \nabla\cdot(D(\boldsymbol{x})\nabla\boldsymbol{M}). \tag{1}$$

This equation describes the time evolution of the complex-valued, transverse spin magnetization ($\boldsymbol{M}$) resulting from an externally applied, spatially and temporally varying magnetic field ($\boldsymbol{G}(t)\cdot\boldsymbol{x}$). Here i is the imaginary unit, γ is the gyromagnetic ratio of ^1H, $\boldsymbol{x}$ is the spin position vector, $\boldsymbol{G}(t)$ is the time-varying magnetic field gradient vector used to encode diffusion, T_2 is the spin-spin relaxation time, and $D(\boldsymbol{x})$ is the local diffusion coefficient. The dMRI signal is expressed by the following integral over (typically) the voxel volume,

$$S(t) = \int_V |\boldsymbol{M}(\boldsymbol{x},t)| d\boldsymbol{x}. \tag{2}$$

Optimizing a dMRI pulse sequence involves adjusting its parameters to sensitize the signal to desired properties of the microstructure. While advanced sequences exist to extract more complex information from the tissue [14–16], here we focus on the standard pulsed-gradient spin echo (PGSE) sequence [17] which can be described by three parameters: gradient duration (δ), gradient vector ($\boldsymbol{g}$), and diffusion time (Δ) (cf. Figure 1a). Diffusion-weighting results in increased attenuation of the signal in areas with higher diffusion coefficients. The signal is normalized by the non-diffusion-weighted signal, S_0, to provide an attenuation ratio, $E(\boldsymbol{q}) = S(\boldsymbol{q})/S_0$, where

$\boldsymbol{q} = \gamma \boldsymbol{g} \delta / 2\pi$. This attenuation ratio is related to the ensemble average propagator (EAP) of the voxel,

$$E(\boldsymbol{q}, \tau) = \int_{\boldsymbol{r} \in \mathbb{R}^3} P(\boldsymbol{r}, \tau) e^{i 2\pi \boldsymbol{q} \cdot \boldsymbol{r}} d\boldsymbol{r}, \tag{3}$$

where $P(\boldsymbol{r}, \boldsymbol{\tau})$ is the EAP, $\boldsymbol{r}$ is the displacement vector, and τ is the diffusion time. The EAP is a two-point probability function of the spin displacement and thus a representation of how microstructural features restrict the diffusion behavior in tissue [18–20]. In the case of unrestricted, Gaussian diffusion in a homogeneous domain, equation 3 can be reduced to

$$E(\boldsymbol{q}, \tau) = e^{4\pi^2 \boldsymbol{q}^\intercal \boldsymbol{D} \boldsymbol{q} \tau}. \tag{4}$$

Here $\boldsymbol{D}$ is the second rank diffusion tensor that describes the apparent diffusion coefficients in the voxel [21]. For a PGSE sequence, $\tau = \Delta - \delta/3$ and is often combined with $\boldsymbol{q}$ to yield the so-called b-value, or b-matrix, $\boldsymbol{b} = (2\pi \boldsymbol{q})^2 (\Delta - \delta/3)$, resulting in the simplified representation: $E(\boldsymbol{q}) = e^{-\boldsymbol{b}:\boldsymbol{D}}$ [21]. In complex tissues containing many barriers, such as muscle, this diffusion tensor is anisotropic and composed of three distinct eigenvalues $(\lambda_1, \lambda_2, \lambda_3)$, which correspond to the principle directions. The eigenvalues can be used to calculate various diffusion metrics such as fractional anisotropy, $FA = \sqrt{\frac{(\lambda_1-\lambda_2)^2+(\lambda_2-\lambda_3)^2+(\lambda_3-\lambda_1)^2}{2(\lambda_1^2+\lambda_2^2+\lambda_3^2)}}$, mean diffusivity, $MD = (\lambda_1 + \lambda_2 + \lambda_3)/3$, and radial diffusivity, $RD = (\lambda_2 + \lambda_3)/2$. These metrics characterize the diffusion rate and tensor anisotropy within the voxel.

Pulse Parameterization

In the present study, the key PGSE sequence parameters focused on are the diffusion time and gradient strength, while the gradient duration is fixed at 5 ms and TE is defined as $\Delta + \delta$. We focus on the effect of diffusion time (Δ) and gradient strength (g) because both affect the resolving ability of dMRI. The EAP is a representation of how microstructural features effect the diffusion behavior within tissue, however, the EAP is dependent on the diffusion time used in the dMRI experiment. As the diffusion time increases, the average displacement of spins increases, allowing them to interact with microstructural features further away from their original location. This effect of diffusion time has been used to estimate cell diameter in both muscle and axons [14, 22, 23].

Because the EAP is the inverse Fourier transform of the signal attenuation, measuring it at different q-values allows sampling its shape [24]. By fixing the gradient duration, the gradient strength directly relates to the q-value. When Gaussian diffusion is assumed, only one q-value is necessary [25]. Under this assumption the computed diffusion tensor and related dMRI indices should not change for different gradient strengths. Varying the gradient strength allows checking the appropriateness of the Gaussian diffusion assumption. The key idea behind focusing on

diffusion time and gradient strength is that diffusion time defines the EAP, while gradient strength, more specifically q-value, determines the sampling of the EAP.

Myocyte Tissue Model

To model the effect of skeletal muscle microstructure on the dMRI signal, it is first necessary to create a model with parameterized microstructural features. Skeletal muscle has a hierarchical order, exhibiting a long-range order of parallel, elongated cells, each surrounded by a semi-permeable membrane and embedded in an extracellular matrix made up of collagen fibers. This organization allows use of a simplified skeletal muscle model consisting of infinitely long, parallel cylinders packed in a periodic hexagonal array (Figure 1b). This periodic packing allows the definition of a representative elemental volume (REV), as shown in Figure 1b. By restricting our computational to a single REV, we can economically parameterize the domain and consider how microstructural changes effect the dMRI signal. Such an investigation obviously ignores the typical variations of structural parameters, such as fiber size [10], within a voxel. However, considering a periodic domain is a necessary first step to understanding how individual parameters behave before including such confounding factors as cell size distributions.

The REV is defined by seven parameters: intra- and extra-cellular diffusion coefficients, cell diameter, packing fraction, membrane permeability and intra- and extra-cellular T_2 relaxation time. The intra- and extra-cellular domains both contain sub-cellular structures which restrict the free diffusion of water, however, such restrictions cannot be modeled at the current spatial scale so they are accounted for through the use of effective diffusion coefficients (D_{in} and D_{ex}) [26].

While the present periodic model accounts for isotropic transverse diffusion, muscle exhibits transversely anisotropic diffusion [26, 27]. The source of this transverse anisotropy is not conclusively known, so this factor is set aside for now. Solutions for the dMRI signal in simplified geometrical domains is known analytically [28, 29], and progress has been made on more complex geometries [30], however, solutions for heterogeneous domains of embedded, tightly packed cells, such as those considered here, do not exist, necessitating a numerical solution of dMRI in the tissue.

Numerical Methods

In this work we solve the Bloch-Torrey equation using the lattice Boltzmann method (LBM) on a D3Q7 stencil. This stencil corresponds to three dimensions and seven lattice directions (speeds). Full details of the implementation are presented in [31] and only a rudimentary description is given below. LBM is a mesoscale numerical scheme, employed here to simulate transport of the complex-valued transverse magnetization on a discrete grid as $\boldsymbol{M}(\boldsymbol{x}, t) = \sum_{i=0}^{6} \boldsymbol{g}_i(\boldsymbol{x}, t)$, where $\boldsymbol{g}_i(\boldsymbol{x}, t)$ is the complex spin probability distribution function representing the two components

of the transverse magnetization vector. Using the Bhatnagar-Gross-Krook collision model with a single relaxation factor (τ), the evaluation of $\boldsymbol{g}_i$ is approximated by a diffusion step,

$$\boldsymbol{g}_i'(\boldsymbol{x} + \boldsymbol{e}_i \cdot \delta x, t) - \boldsymbol{g}_i(\boldsymbol{x}, t) = -\frac{1}{\tau}\left[\boldsymbol{g}_i(\boldsymbol{x}, t) - \boldsymbol{g}_i^{eq}(\boldsymbol{x}, t)\right], \tag{5}$$

followed by a reaction step,

$$\boldsymbol{g}_i(\boldsymbol{x}, t + \delta t) = \exp\left(-\frac{\delta t}{T_2} - i\gamma G^n \boldsymbol{x}_i \delta t\right) \boldsymbol{g}_i'(\boldsymbol{x}, t). \tag{6}$$

where δx and δt are the lattice spacing and time step respectively and $\boldsymbol{e}_i$ represents the lattice speeds. Intra-domain boundary conditions handle the effect of the semi-permeable sarcolemma membrane while modified periodic boundary conditions account for the non-periodic magnetization accumulation over the periodic geometry of the REV. Because the muscle tissue is modeled as a unidirectional composite with infinite cylindrical fibers in the axial direction, translational symmetry allows the use of a single node in that direction.

The numerical grid size is based on geometrical parameters. A node spacing of δx = 0.5 μm is used for the default grid and refined until at least four nodes span the extracellular space. In the lattice Boltzmann method, the time step is related to the grid size through the relaxation factor (τ) and diffusion coefficient (D), $\delta t = \epsilon_D \, \delta x^2(\tau - 0.5)/D$, where ϵ_D = 1/4 for a D3Q7 stencil. Because there are two different diffusion coefficients (intra- and extracellular), the average of the two is used to define the time step with $\tau = 0.95$. This relaxation factor value is used because it minimizes the numerical error in a homogeneous domain (see supplementary information, Figure S1). The signal of the REV is calculated at time t = TE via equation 2.

For each simulation, six gradient directions and a non-diffusion weighted acquisition are simulated [32], and the signal attenuation, $E(\boldsymbol{q})$, is computed. To account for the effect of noise, Rician noise is added to $E(\boldsymbol{q})$ for SNR levels of 100 and 50. Noisy signal is simulated by adding zero mean, unit-variance Gaussian noise, dividing by a scaling factor, adding this noise to both real (n_r) and imaginary (n_i) components of $E(\boldsymbol{q})$, and taking the norm of the resulting signal, $E(\boldsymbol{q})_{SNR} = |E(\boldsymbol{q}) + n_r + in_i|$ [8, 33]. Two version of the noisy signal are computed, the first with no averaging and the second as the average of adding noise ten separate times. These resulting signals were fit to a diffusion tenor using the fanDTasia ToolBox [34]. From the diffusion tensor, FA, MD, RD and the tensor eigenvalues ($\lambda_1, \lambda_2, \lambda_3$) are calculated.

Global Sensitivity Analysis

To determine how changes in microstructure and pulse parameters affect the dMRI signal, a global sensitivity analysis was performed, which characterizes how changes to the input

parameters effect the variance of the model's output, while making no assumptions about the relationship between inputs and outputs [35]. The analysis decomposes the variance of the model's output into the variances of the individual input parameters and combinations of inputs. This allows the determination of the contribution of each input parameter, as well as their interactions, to the variance of the model output (FA, MD, etc.). We use the method developed by Saltelli et al. [36, 37] as implemented in the open source SaLib python package [38]. Reviews of this method have been presented elsewhere [39, 40].

This method computes the first, second and total-order sensitivity indices of the input parameters. First-order sensitivity indices describe the fraction of the total variance of the output attributed to a particular parameter. For example, a first-order volume fraction sensitivity index of 0.50 for FA would mean that 50% of the total variance in FA can be described by volume fraction changes alone. Second-order indices denote how the interaction of two parameters contributes to the total output variance and total-order indices are the sum of first, second, and higher order indices for each parameter. Parameters are sampled independently from a uniform distribution of values within a range. The total number of model evaluations is $2N(p+1)$, where p is the number of parameters and N is the number of independent samples of each parameter.

Microstructural parameter ranges were determined from reported literature values and are presented in Table 1. Pulse parameters are also presented in Table 1. These pulse parameters are typical for dMRI sequences performed on clinical scanners. We note in passing that the combination of the upper end of the diffusion time and gradient strength correspond to b-values that can result in dMRI signal with too low a SNR to measure in muscle (Δ = 750 ms, g = 80 mT/m $\rightarrow$ b = 6568 s/mm^2). Muscle has a short T_2, which requires the implementation of stimulated echo (STEAM) sequences for long diffusion times [22, 41]. STEAM sequences are not considered here; instead, the simplified PGSE pulse was used for all simulations.

Parameter sampling was preformed using the Sobol scheme, which is a quasi-random, low discrepancy method that allows more uniform coverage of the input parameter space than traditional Monte Carlo methods [36, 42]. 5,000 samples were taken for each of the nine parameters for a total of 100,000 parameter sets. These parameter sets defined the microstructural domain and PGSE pulse sequence for which the Bloch-Torrey equation was numerically solved with the lattice Boltzmann method. The resulting signals were used to calculate FA, MD, RD and the tensor eigenvalues. A sensitivity analysis was performed for all six dMRI metrics for both noise-free simulations and the two SNR levels both with and without averaging of the added noise.

3 Results

The computations for the sensitivity analysis were performed on the San Diego Supercomputing Center's Comet cluster [43] which consists of nodes with 2 x 12 core CPU processors (Intel Xeon E5-2680 v3 2.5 Ghz), and 128 GB DDR4 DRAM running CentOS 6.7. 40 nodes were used to run three simulations simultaneously on each node, with each simulation using 8 cores. The computer simulations for the entire study took approximately 7000 core hours. The numerical results were post-processed to calculate the diffusion tensor and six dMRI metrics. For each of the dMRI metrics (FA, MD, RD, λ_1, λ_3, and λ_3) and each noise level, a separate sensitivity analysis was performed. A comparison of the noise-free sensitivity indices and the indices for SNR = 50 with both no averaging and averaging is shown in Figure 2. The comparison for SNR = 100 is shown in Figure 3. Non-zero second-order indices for noise free results are given in Table 2. Additional results from the sensitivity analysis are available in the supplementary information section.

4 Discussion

Effect of Synthetic Noise

The goal of this sensitivity study is to identify the affect of microstructural and PGSE pulse parameters on dMRI measurements. An important additional consideration is how noise affects this relationship, so we begin by examining the effect synthetic noise has on the sensitivity indices. Focusing on the first-order indices, Figures 2a and 3a indicate that the largest effect of adding noise is the decrease in sensitivity of MD and λ_1 to both diffusion coefficients, as well as an increase in sensitivity to gradient strength and diffusion time. Though the effect is stronger for lower SNR, these changes occur for both SNR levels. Additionally, adding noise decreases FA's sensitivity to diffusion time. It also decreases the sensitivity of RD, λ_2, and λ_3 to diameter, permeability, and both diffusion coefficients, although much of this change is within the confidence intervals. Comparing sensitivity indices with and without averaging, one sees that not averaging yields a decrease in first-order sensitivity to the majority of the microstructural parameters for all dMRI metrics. However, averaging the signal over the different realizations generally results in indices that are much closer to the noise free results. This result illustrates the importance of averaging dMRI measurements if the intent is to use them to infer microstructural properties. The difference with and without averaging is most pronounced for lower SNR level, although it is still noticeable for SNR of 100.

Turning to the total-order indices, the effect of noise shown in Figures 2b and 3b is similar to that seen for the first-order indices because total-order indices include the contribution of first-order indices. One notable difference is the effect on FA of adding SNR without averaging.

In this case, the sensitivity indices are consistently higher than the noise-free indices, however, this effect disappears when averaging is performed. A similar, but weaker, effect occurs to λ_1, λ_2, and λ_3 for all microstructural parameters. Finally, adding noise increases the sensitivity to gradient strength and diffusion time. Overall, the largest effect of adding noise, particularly when averaging is performed, is the decrease in sensitivity to intracellular and extracellular diffusion coefficients and the concomitant increase in sensitivity to gradient strength and diffusion time.

PGSE Pulse Parameters

Focusing more closely on pulse parameters, we first consider the noise-free results. FA, RD, λ_2 and λ_3 are all sensitive to diffusion time, while λ_1 and MD are not. The same holds for gradient strength, but to a lesser degree. The lack of sensitivity of λ_1 to these pulse parameters is expected. Our simplified model has no restrictions to diffusion in the axial direction, so the Gaussian assumption used in calculating the diffusion tensor is correct. In the radial direction, however, diffusion is restricted due to the finite permeability of cell membranes. As the diffusion time increases, more interior spins interact with these membranes, leading to non-Gaussian transverse diffusion and sensitivity to diffusion time. This non-Gaussian behavior is also reflected in the dependence on gradient strength. Changing gradient strength leads to sampling the EAP, which is non-Gaussian in the radial direction, at different q-values. When reporting muscle dMRI results, it is important to report both diffusion time and gradient strength as both independently effect radial diffusion; reporting only a b-value is not sufficient [25].

Adding noise increases the sensitivity of the model to both gradient strength and diffusion time, particularly in terms of the total-order indices. A possible explanation for this increase is that gradient and diffusion time are the parameters that most directly effect the magnitude of $\mathrm{E}(\boldsymbol{q})$. Longer diffusion time and higher gradient strength both cause smaller $\mathrm{E}(\boldsymbol{q})$, leading to a more pronounced effect of noise. This also explains why λ_1 is the parameter most affected by noise because $\mathrm{E}(\boldsymbol{q})$ is always lowest in the λ_1 direction. The effect of noise on $\mathrm{E}(\boldsymbol{q})$ leads to errors in fitting the diffusion tensor which, in turn, affects all computed dMRI metrics. Minimum SNR levels of 40-60 have been suggested for muscle DTI [8]; our results suggest that adding noise at such levels does not preclude the interpretation of muscle dMRI in terms of its underlying microstructure, though care must be taken in assuring appropriate averaging is preformed.

Microstructural Parameters

Next, we consider the sensitivity indices of the microstructural parameters. Our results give insight into which microstructural features are important to consider and which can be ignored. The diffusion coefficients for the intra- and extracellular domains have the largest first-order effect on all parameters except FA. These diffusion coefficients form the basis of the measured

diffusion tensor so their strong influence is unsurprising. Similarly, FA is a ratio of eigenvalues so the effect of diffusion coefficients is weakened. These effective diffusion coefficients represent the cumulative effects of sub-cellular restrictions. The results of Winters et al. [6] indicate that there is a time dependence in the λ_1 direction, which may relate to structures such as z-disk or sarcomere spacing, so there may be additional structural information available in these effective compartmental diffusion coefficients which was not considered here.

After the diffusion coefficients, the next most sensitive microstructural parameter is cell diameter, though it only effects metrics heavily influenced by radial diffusion (FA, RD, λ_2, and λ_3). The affect of cell diameter on radial diffusion has been illustrated previously [22, 44], and these current results bolster the claim that diameter can be inferred from the dMRI signal. The final microstructural parameter that has a substantial first-order effect is permeability, although, again, only in the radial direction.

Two parameters that have little to no influence are the T_2 relaxation values. Many models of dMRI in muscle do not consider the effects of T_2 [45–47], with the rationale that T_2 effects disappear when normalizing by the non-diffusion weighted signal. There is a large difference in the intra and extracellular diffusion coefficients, so it is not possible to completely factor out the two different T_2 effects. This difference does influence the signal behavior as permeability increases [9, 48], however, our results suggest that this effect is minimal when compared with the effects of other microstructural parameters. So the present results indicate that T_2 effects are not necessary to model in dMRI of skeletal muscle.

Second-Order Indices

Looking at the second-order indices for the noise-free results, Table 2 shows that only four indices have a noticeable effect. These are diameter & volume fraction, diameter & intracellular diffusion coefficient, volume fraction & extracellular diffusion coefficient, and volume fraction & intracellular diffusion coefficient. These four combinations can each be related to key microstructural parameters. Diameter & volume fraction define the extracellular length scale while diameter & intracellular diffusion coefficient is related to the intracellular diffusion distance necessary to encounter diffusion barriers such as the cell membrane. For the primary eigenvalue, the combination of the volume fraction and diffusion coefficients reflects the notion that λ_1 is the sum of the volume-weighted components of free diffusion in the axial direction.

In the radial direction (RD, λ_2 and λ_3), volume fraction & diameter again describe the extracellular length scale and the extent to which extracellular diffusion is hindered, while volume fraction & the extracellular diffusion coefficient give a measure of how easily the spins can move through this hindered extracellular space. An interesting result of examining these second-order

indices is that even though volume fraction has low first-order sensitivity, it has a noticeable effect when combined with other parameters. It is noteworthy that even in these densely packed cell arrangements, the extracellular space has a significant effect on the signal. This suggests that it should be possible to extract extracellular information from dMRI measurements.

Comparison with Prior Studies

Comparing these results with those reported by prior studies, we note a number of similarities and differences. Hall and Clark [10] and Berry et al. [11] did not examine the role of the diffusion coefficient, and Bates et al. [12] kept both intra and extracellular diffusion coefficients the same. Our results suggest that both intra and extracellular effective diffusion coefficients have a substantial effect on dMRI signal. Some models of muscle dMRI only use one diffusion coefficient to represent the entire muscle [10–12, 22, 45], however, the histoarchitectures of the intra- and extracellular regimes are substantially different. The extracellular space consists of a collagen fiber matrix, while the intracellular space contains myofibrils, sarcoplasmic reticuli, mitochondria, t-tubles and cell nuclei. There is no reason to assume that these restrictions lead to similar effective diffusion coefficients. In fact, preliminary evidence suggests that muscle consists of multiple pools of diffusion coefficients [49]. Since both coefficients substantially affect the signal, further investigation is needed to determine how different these effective diffusion coefficients are and if it is appropriate to combine them into a single coefficient. The effect of subcellular structures on the effective diffusion coefficients points to limitation of the simplified structural model of muscle used here, especially in modeling axial diffusion. Future improvements of the tissue model will do well to incorporate the effect of subcellular structures such as sarcomere length [6], or myofibril distribution [10] on the determination of effective diffusion coefficients.

The differences between prior results and the present study extend to permeability and diameter as well, which were considered by Hall and Clark [50] and Berry et al. [11] but with disparate results. Hall and Clark examined the change in entropy of the signal and found that permeability has the largest effect on this measure. Berry et al. found that fiber diameter has a larger effect. Our results agree with Berry et al, although we find that diameter has a stronger relative effect compared to permeability than they report. A caveat in comparing these results is the difference in model setup. Hall and Clark used a muscle tissue model consisting of cylinders embedded in larger cylinders and considered a impermeable baseline case. These embedded cylinders are more representative of myofibrils than myocytes. As such, the change in permeability of these embedded cylinders compares more directly to a change in the effective intracellular diffusion coefficients in our model, in which case our results agree with theirs. Berry et al. modify the permeability of the myocytes by randomly deleting the cell wall of a portion of the

cells in the domain, leading to completely permeable cells. This is in contrast to our use of a semi-permeable membrane on all cells and may explain the differences in results. We model membrane permeability as a change in flux. This treatment more closely relates to membrane damage found in dystrophin-deficient muscle [4, 5] and muscle metabolism [6]. Bates et al. also model permeability in this way, but do not systematically examine its effect.

Another key difference with previous studies is the treatment of pulse parameters. Berry et al. examine a single diffusion time and gradient strength. Bates et al. considers these parameters individually, although their sensitivity analysis is performed at a single diffusion time and gradient strength. Hall and Clark examine the parameter space of diffusion time and gradient strength but use them as fixed parameters in their study. In contrast, we treat diffusion time and gradient strength as input parameters to the sensitivity analysis. This allows a comparison of the effects these parameters have on the dMRI signal relative to the microstructural effects.

Comparing sensitivity results as a whole, the present results agree most closely with Berry et al. and Bates et al. They do not agree with Hall and Clark, likely due to the tissue model differences mentioned above. Our general agreement with Berry et al. and Bates et al. is notable; they both perform their analysis using relatively short diffusion times (9 and 7 ms respectively) while we consider a much larger range of diffusion times and gradient strengths. This similarity suggests that the influence of individual parameters does not change for different diffusion time and gradient strengths, a point further supported by the lack of significant second-order sensitivity indices related to diffusion time or gradient strength.

Usefulness of Sensitivity Indices

Sensitivity indices are only meaningful if the parameter ranges are realistic. The sensitivity indices are global indices and describe the effect over the prescribed range as a whole. If a parameter actually has a much smaller or larger range, this will change its effect on the dRMI signal. The parameter ranges chosen are intentionally broad to include the majority of values reported in the literature. Additional measurements will allow refining these parameter ranges leading to more accurate sensitivity indices. Despite this uncertainty, the results presented here can still help identify important microstructural parameters to control for. For example, if one wishes to measure permeability, diffusion coefficients need to be carefully estimated, since any change in them could easily overwhelm any measured change in permeability. Another possible use of these results is in making comparisons between dMRI metrics. As an example, if an experiment measures a difference in MD but not in FA (like that reported between athletes and non-athletes [51]), then this is unlikely to be caused by changes in diameter or permeability, as both of these have higher sensitivity to FA than MD. Rather, it is likely that intra and extracellular

diffusion coefficients are better candidates to explain such a difference as they have small impact on FA but a much larger one on MD. Such an analysis does not conclusively prove the effect of a microstructural parameter, but does help identify candidates and rule out others for further investigation.

5 Conclusion

The goal of this study is to determine which microstructural parameters most influence muscle dMRI signal over a wide range of possible PGSE pulse sequences. We performed a global sensitivity analysis of the effect microstructural and PGSE pulse parameters have on dMRI metrics of FA, MD, RD and the diffusion tensor eigenvalues. We examined the effect that adding synthetic noise (SNR levels of 50 and 100 both with and without averaging), have on the sensitivity indices. We conclude that the effect of noise is important, but that averaging mitigates its effect. We find that diffusion time and gradient strength are important independently, and therefore, both should be reported in dMRI experiments. We report that diffusion coefficients have the largest effect on the examined microstructural parameters, and that diameter is more influential than permeability in the transverse direction. We also conclude that dMRI is sensitive to extracellular parameters suggesting that such extracellular information can be extracted by solving the corresponding inverse problems. By identifying the key microstructural features that affect dMRI measurements, the present sensitivity results can help interpret dMRI signal measurements and inform further model development by reducing the number of microstructural parameters considered, such as intra- and extracellular T_2.

Acknowledgments

This work used the Extreme Science and Engineering Discovery Environment (XSEDE), which is supported by National Science Foundation grant number ACI-1548562. Additional support was provided by the R.A. Pritzker endowed chair and NSF grants CBET-1236451 and CMI-1762774 as well as an NSF GRFP award for N. Naughton.

Supporting Information

Figure S1: Relative error of LBM model solved over a homogeneous domain for different relaxation factors.

Table S1: Table of all first- and total-order sensitivity indices as well as all non-zero second-order indices. Bold denotes a value higher than 0.05.

References

[1] Mann CJ, Perdiguero E, Kharraz Y, Aguilar S, Pessina P, Serrano AL, et al. Aberrant repair and fibrosis development in skeletal muscle. Skeletal Muscle 2011;1(1):21.

[2] Kirkendall DT, Garrett WE. The effects of aging and training on skeletal muscle. The American Journal of Sports Medicine 1998;26(4):598–602.

[3] Tieland M, Trouwborst I, Clark BC. Skeletal muscle performance and ageing. Journal of Cachexia, Sarcopenia and Muscle 2018;9(1):3–19.

[4] Brussee V, Tardif F, Tremblay JP. Muscle fibers of mdx mice are more vulnerable to exercise than those of normal mice. Neuromuscular Disorders 1997;7(8):487–492.

[5] Petrof BJ, Shrager JB, Stedman HH, Kelly AM, Sweeney HL. Dystrophin protects the sarcolemma from stresses developed during muscle contraction. Proceedings of the National Academy of Sciences 1993;90(8):3710–3714.

[6] Winters KV, Reynaud O, Novikov DS, Fieremans E, Kim SG. Quantifying myofiber integrity using diffusion MRI and random permeable barrier modeling in skeletal muscle growth and Duchenne muscular dystrophy model in mice. Magnetic Resonance in Medicine 2018;http://doi.wiley.com/10.1002/mrm.27188.

[7] Jelescu IO, Budde MD. Design and validation of diffusion MRI models of white matter. Frontiers in Physics 2017;5:61.

[8] Damon BM. Effects of image noise in muscle diffusion tensor (DT)-MRI assessed using numerical simulations. Magnetic Resonance in Medicine 2008;60(4):934–944. http://doi.wiley.com/10.1002/mrm.21707.

[9] Naughton NM, Georgiadis JG. Comparison of two-compartment exchange and continuum models of dMRI in skeletal muscle. Physics in Medicine and Biology 2019 (in revision);Preprint available at https://git.io/fjqQH.

[10] Hall MG, Clark CA. Diffusion in hierarchical systems: A simulation study in models of healthy and diseased muscle tissue. Magnetic Resonance in Medicine 2017;78(3):1187–1198. http://doi.wiley.com/10.1002/mrm.26469.

[11] Berry DB, Regner B, Galinsky V, Ward SR, Frank LR. Relationships between tissue microstructure and the diffusion tensor in simulated skeletal muscle. Magnetic Resonance in Medicine 2018;80(1):317–329. http://doi.wiley.com/10.1002/mrm.26993.

[12] Bates J, Teh I, McClymont D, Kohl P, Schneider JE, Grau V. Monte Carlo Simulations of Diffusion Weighted MRI in Myocardium: Validation and Sensitivity Analysis. IEEE Transactions on Medical Imaging 2017;36(6):1316–1325. http://ieeexplore.ieee.org/document/7875442/.

[13] Torrey HC. Bloch equations with diffusion terms. Physical Review 1956;104(3):563.

[14] Nilsson M, Lasič S, Drobnjak I, Topgaard D, Westin CF. Resolution limit of cylinder diameter estimation by diffusion MRI: The impact of gradient waveform and orientation dispersion. NMR in Biomedicine 2017;30(7):e3711. http://doi.wiley.com/10.1002/nbm.3711.

[15] Mitra PP. Multiple wave-vector extensions of the NMR pulsed-field-gradient spin-echo diffusion measurement. Physical Review B 1995;51(21). https://journals.aps.org/prb/pdf/10.1103/PhysRevB.51.15074.

[16] Drobnjak I, Siow B, Alexander DC. Optimizing gradient waveforms for microstructure sensitivity in diffusion-weighted MR. Journal of Magnetic Resonance 2010;206(1):41–51.

[17] Stejskal EO, Tanner JE. Spin diffusion measurements: spin echoes in the presence of a time-dependent field gradient. The Journal of Chemical Physics 1965;42(1):288–292.

[18] Kärger J, Heink W. The propagator representation of molecular transport in microporous crystallites. Journal of Magnetic Resonance (1969) 1983;51(1):1–7.

[19] Callaghan PT. Principles of nuclear magnetic resonance microscopy. Oxford University Press on Demand; 1993.

[20] Assemlal HE, Tschumperlé D, Brun L, Siddiqi K. Recent advances in diffusion MRI modeling: Angular and radial reconstruction. Medical Image Analysis 2011;15(4):369–396.

[21] Basser PJ. Relationships between diffusion tensor and q-space MRI. Magnetic Resonance in Medicine 2002;47(2):392–397.

[22] Fieremans E, Lemberskiy G, Veraart J, Sigmund EE, Gyftopoulos S, Novikov DS. In vivo measurement of membrane permeability and myofiber size in human muscle using time-dependent diffusion tensor imaging and the random permeable barrier model. NMR in Biomedicine 2017;30(3).

[23] Xu J, Does MD, Gore JC. Quantitative characterization of tissue microstructure with temporal diffusion spectroscopy. Journal of Magnetic Resonance 2009;200(2):189–197. http://dx.doi.org/10.1016/j.jmr.2009.06.022.

[24] Descoteaux M, Deriche R, Le Bihan D, Mangin JF, Poupon C. Multiple q-shell diffusion propagator imaging. Medical Image Analysis 2011;15(4):603–621.

[25] Grebenkov DS. Use, misuse, and abuse of apparent diffusion coefficients. Concepts in Magnetic Resonance Part A: An Educational Journal 2010;36(1):24–35.

[26] Galban CJ, Maderwald S, Uffmann K, de Greiff A, Ladd ME. Diffusive sensitivity to muscle architecture: a magnetic resonance diffusion tensor imaging study of the human calf. European Journal of Applied Physiology 2004;93(3):253–262.

[27] Karampinos DC, King KF, Sutton BP, Georgiadis JG. Myofiber ellipticity as an explanation for transverse asymmetry of skeletal muscle diffusion MRI in vivo signal. Annals of Biomedical Engineering 2009;37(12):2532–2546.

[28] Tanner JE, Stejskal EO. Restricted self-diffusion of protons in colloidal systems by the pulsed-gradient, spin-echo method. The Journal of Chemical Physics 1968;49(4):1768–1777.

[29] Söderman O, Jönsson B. Restricted diffusion in cylindrical geometry. Journal of Magnetic Resonance, Series A 1995;117(1):94–97.

[30] Grebenkov DS. Pulsed-gradient spin-echo monitoring of restricted diffusion in multilayered structures. Journal of Magnetic Resonance 2010;205(2):181–195.

[31] Naughton NM, Tennyson CG, Georgiadis JG. Lattice Boltzmann method for simulation of diffusion magnetic resonance imaging physics in heterogeneous tissue models. Journal of Computational Physics 2019 (submitted);Preprint available at https://git.io/fhodg.

[32] Hasan KM, Parker DL, Alexander AL. Comparison of gradient encoding schemes for diffusion-tensor MRI. Journal of Magnetic Resonance Imaging 2001;13(5):769–780.

[33] Gudbjartsson H, Patz S. The Rician distribution of noisy MRI data. Magnetic Resonance in Medicine 1995;34(6):910–914.

[34] Barmpoutis A, Vemuri BC. A unified framework for estimating diffusion tensors of any order with symmetric positive-definite constraints. In: Biomedical Imaging: From Nano to Macro, 2010 IEEE International Symposium on IEEE; 2010. p. 1385–1388.

[35] Sobol IM. Global sensitivity indices for nonlinear mathematical models and their Monte Carlo estimates. Mathematics and Computers in Simulation 2001;55(1-3):271–280.

[36] Saltelli A. Making best use of model evaluations to compute sensitivity indices. Computer Physics Communications 2002;145(2):280–297.

[37] Saltelli A, Annoni P, Azzini I, Campolongo F, Ratto M, Tarantola S. Variance based sensitivity analysis of model output. Design and estimator for the total sensitivity index. Computer Physics Communications 2010;181(2):259–270.

[38] Herman J, Usher W. SALib: an open-source Python library for sensitivity analysis. The Journal of Open Source Software 2017;2(9).

[39] Saltelli A, Ratto M, Andres T, Campolongo F, Cariboni J, Gatelli D, et al. Global sensitivity analysis: the primer. John Wiley & Sons; 2008.

[40] Zhang XY, Trame M, Lesko L, Schmidt S. Sobol sensitivity analysis: a tool to guide the development and evaluation of systems pharmacology models. CPT: Pharmacometrics & Systems Pharmacology 2015;4(2):69–79.

[41] Sigmund EE, Novikov DS, Sui D, Ukpebor O, Baete S, Babb JS, et al. Time-dependent diffusion in skeletal muscle with the random permeable barrier model (RPBM): application to normal controls and chronic exertional compartment syndrome patients. NMR in Biomedicine 2014;27(5):519–528.

[42] Sobol' IM. On the distribution of points in a cube and the approximate evaluation of integrals. Zhurnal Vychislitel'noi Matematiki i Matematicheskoi Fiziki 1967;7(4):784–802.

[43] Towns J, Cockerill T, Dahan M, Foster I, Gaither K, Grimshaw A, et al. XSEDE: Accelerating Scientific Discovery. Computing in Science & Engineering 2014;16(5):62–74. doi.ieeecomputersociety.org/10.1109/MCSE.2014.80.

[44] Li H, Jiang X, Xie J, McIntyre JO, Gore JC, Xu J. Time-dependent influence of cell membrane permeability on MR diffusion measurements. Magnetic Resonance in Medicine 2016;75(5):1927–1934.

[45] Galbán CJ, Maderwald S, Uffmann K, de Greiff A, Ladd ME. Diffusive sensitivity to muscle architecture: a magnetic resonance diffusion tensor imaging study of the human calf. European Journal of Applied Physiology 2004;93(3):253–262. http://link.springer.com/10.1007/s00421-004-1186-2.

[46] Laghi L, Venturi L, Dellarosa N, Petracci M. Water diffusion to assess meat microstructure. Food Chemistry 2017;236:15–20. https://www.sciencedirect.com/science/article/pii/S0308814616320520.

[47] Fieremans E, Lemberskiy G, Veraart J, Sigmund EE, Gyftopoulos S, Novikov DS. In vivo measurement of membrane permeability and myofiber size in human muscle using time-dependent diffusion tensor imaging and the random permeable barrier model. NMR in Biomedicine 2017;30(3):e3612. http://doi.wiley.com/10.1002/nbm.3612.

[48] Harkins KD, Galons JP, Secomb TW, Trouard TP. Assessment of the effects of cellular tissue properties on ADC measurements by numerical simulation of water diffusion. Magnetic Resonance in Medicine 2009;62(6):1414–1422.

[49] Helmer KG, Seland JG, Henninger N, Sotak CH. Separation of the Intra- and Extracellular Apparent Diffusion Coefficients (ADC) of Water in Rat Skeletal Muscle using Spectroscopic MEMRI. In: Proceedings of the Annual Meeting of the International Society for Magnetic Resonance in Medicine;. .

[50] Hall MG, Clark CA. Diffusion in hierarchical systems: A simulation study in models of healthy and diseased muscle tissue. Magnetic Resonance in Medicine 2017;78(3):1187–1198.

[51] Okamoto Y, Kemp GJ, Isobe T, Sato E, Hirano Y, Shoda J, et al. Changes in diffusion tensor imaging (DTI) eigenvalues of skeletal muscle due to hybrid exercise training. Magnetic Resonance Imaging 2014;32(10):1297–1300.

[52] Bolsterlee B, D'Souza A, Gandevia SC, Herbert RD. How does passive lengthening change the architecture of the human medial gastrocnemius muscle? Journal of Applied Physiology 2017;122(4):727–738. http://jap.physiology.org/lookup/doi/10.1152/japplphysiol.00976.2016.

[53] Polgar J, Johnson MA, Weightman D, Appleton D. Data on fibre size in thirty-six human muscles: An autopsy study. Journal of the Neurological Sciences 1973;19(3):307–318. https://www.sciencedirect.com/science/article/pii/0022510X73900944?via{%}3Dihub.

[54] Aliev MK, Tikhonov AN. Obstructed metabolite diffusion within skeletal muscle cells in silico. Molecular and Cellular Biochemistry 2011;358(1-2):105–119.

[55] Porcari P, Hall MG, Clark CA, Greally E, Straub V, Blamire AM. The effects of ageing on mouse muscle microstructure: a comparative study of time-dependent diffusion MRI and histological assessment. NMR in Biomedicine 2018;31(3):e3881. http://doi.wiley.com/10.1002/nbm.3881.

[56] Sigmund EE, Novikov DS, Sui D, Ukpebor O, Baete S, Babb JS, et al. Time-dependent diffusion in skeletal muscle with the random permeable barrier model (RPBM): Application to normal controls and chronic exertional compartment syndrome patients. NMR in Biomedicine 2014;27(5):519–528. http://doi.wiley.com/10.1002/nbm.3087.

[57] Maier F, Bornemann A. Comparison of the muscle fiber diameter and satellite cell frequency in human muscle biopsies. Muscle & Nerve: Official Journal of the American Association of Electrodiagnostic Medicine 1999;22(5):578–583.

[58] Morvan D. In vivo measurement of diffusion and pseudo-diffusion in skeletal muscle at rest and after exercise. Magnetic Resonance Imaging 1995;13(2):193–199.

[59] Vincensini D, Dedieu V, Renou J, Otal P, Joffre F. Measurements of extracellular volume fraction and capillary permeability in tissues using dynamic spin-lattice relaxometry: studies in rabbit muscles. Magnetic Resonance Imaging 2003;21(2):85–93.

[60] Tanner JE. Transient diffusion in a system partitioned by permeable barriers. Application to NMR measurements with a pulsed field gradient. The Journal of Chemical Physics 1978;69(4):1748–1754.

[61] Landis CS, Li X, Telang FW, Molina PE, Palyka I, Vetek G. Equilibrium transcytolemmal water-exchange kinetics in skeletal muscle in vivo. Magnetic Resonance in Medicine 1999;42(3):467–478.

[62] Seland JG, Bruvold M, Anthonsen H, Brurok H, Nordhøy W, Jynge P, et al. Determination of water compartments in rat myocardium using combined D–T1 and T1–T2 experiments. Magnetic Resonance Imaging 2005;23(2):353–354.

[63] Ababneh Z, Beloeil H, Berde CB, Gambarota G, Maier SE, Mulkern RV. Biexponential parameterization of diffusion and T2 relaxation decay curves in a rat muscle edema model: decay curve components and water compartments. Magnetic Resonance in Medicine 2005;54(3):524–531.

[64] Saab G, Thompson RT, Marsh GD. Multicomponent T2 relaxation of in vivo skeletal muscle. Magnetic Resonance in Medicine 1999;42(1):150–157.

[65] Fan RH, Does MD. Compartmental relaxation and diffusion tensor imaging measurements in vivo in λ-carrageenan-induced edema in rat skeletal muscle. NMR in Biomedicine 2008;21(6):566–573. http://doi.wiley.com/10.1002/nbm.1226.

[66] Crémillieux Y, Ding S, Dunn JF. High-resolution in vivo measurements of transverse relaxation times in rats at 7 Tesla. Magnetic Resonance in Medicine 1998;39(2):285–290.

[67] Oudeman J, Nederveen AJ, Strijkers GJ, Maas M, Luijten PR, Froeling M. Techniques and applications of skeletal muscle diffusion tensor imaging: a review. Journal of Magnetic Resonance Imaging 2016;43(4):773–788.

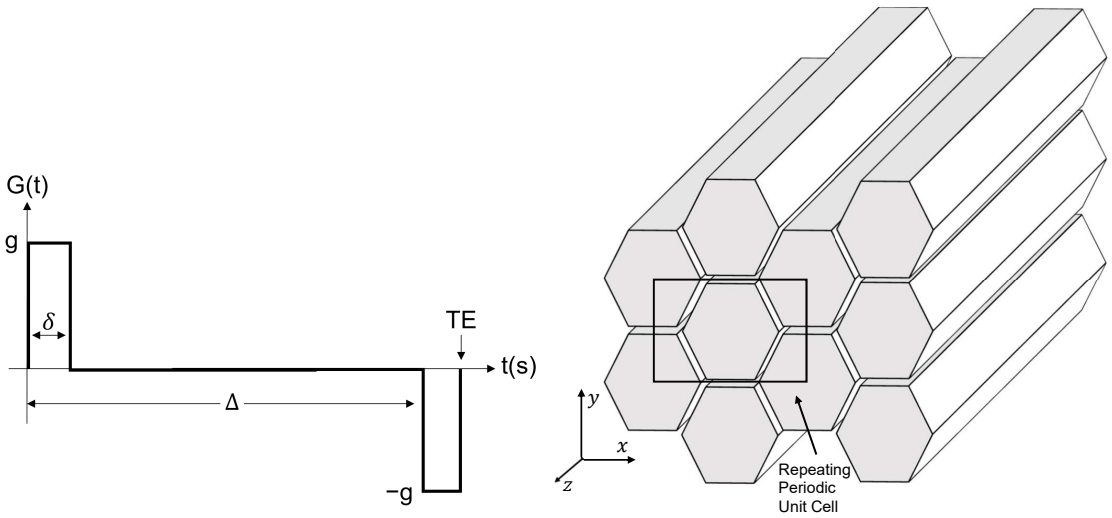

(a) (b)

Figure 1: a) Pulsed Gradient Spin Echo (PGSE) sequence for dMRI and b) periodic muscle fiber model. Solid rectangle designates the representative elementary volume (REV) in the x-y plane.

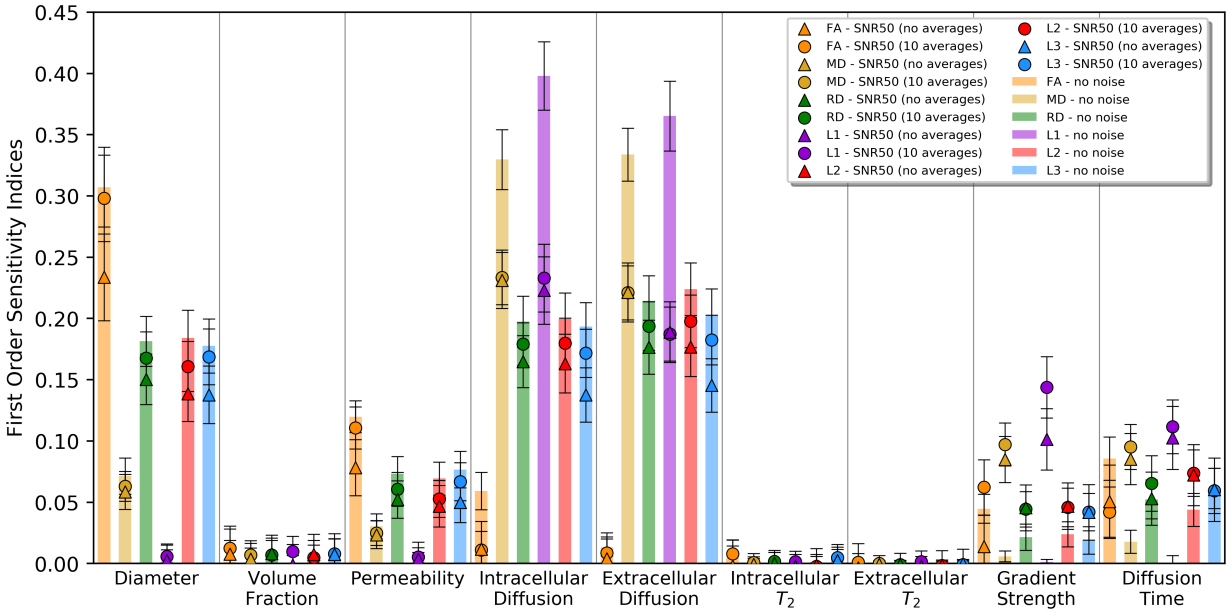

(a)

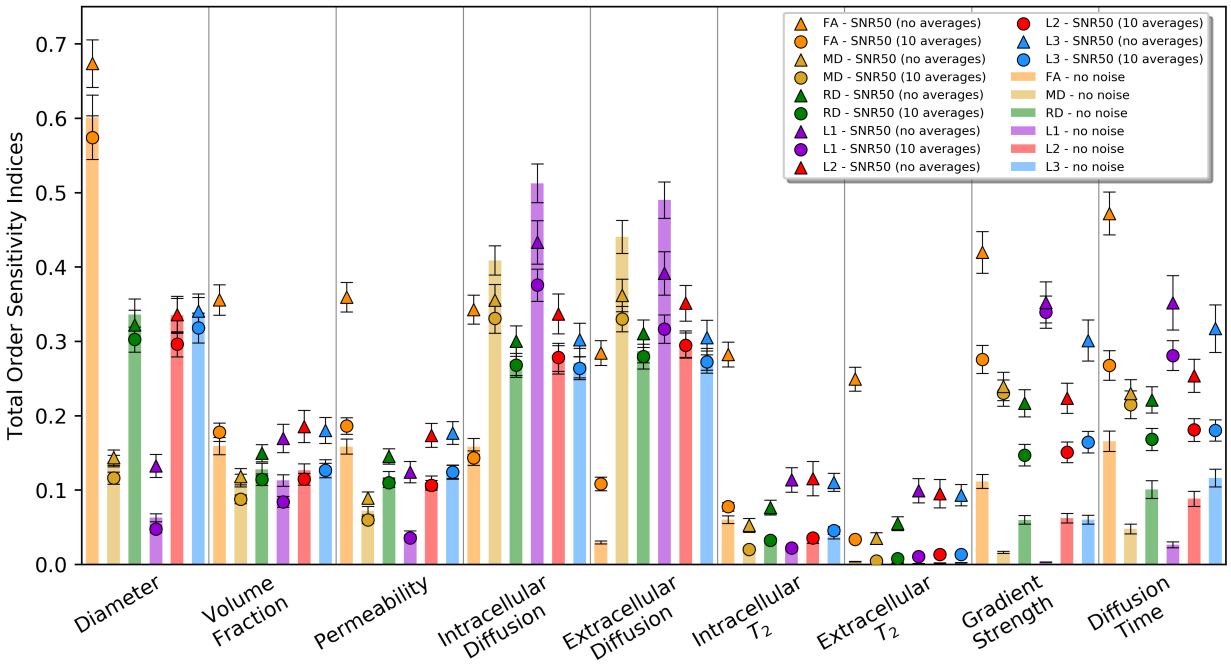

(b)

Figure 2: First-order indices (a) and total-order indices (b) for dMRI signal simulations with no added noise (bar), with added SNR of 50 and no averaging (△), and with SNR of 50 and 10 averages (o). Error bars are confidence intervals.

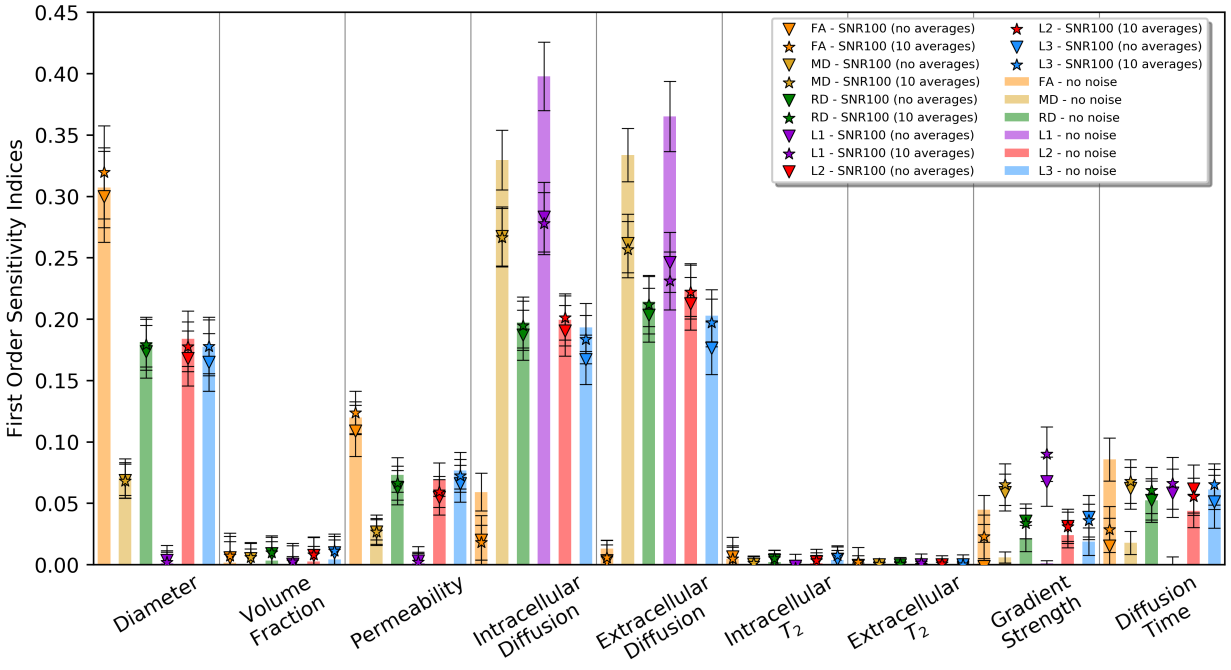

(a)

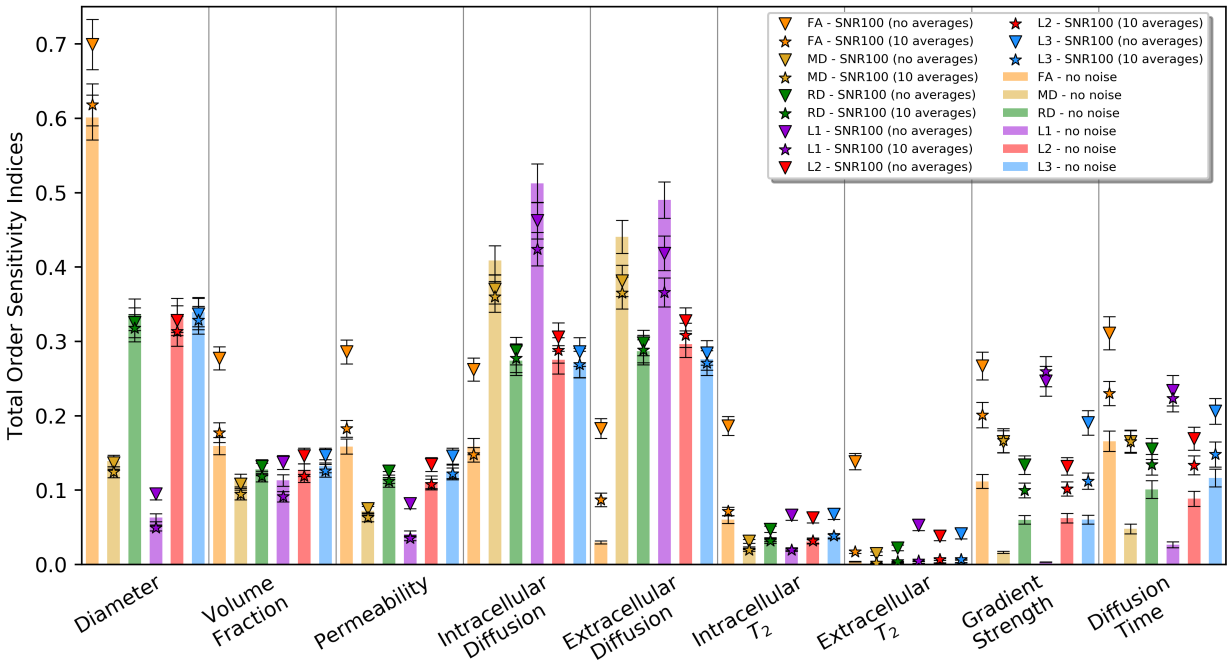

(b)

Figure 3: First-order indices (a) and total-order indices (b) for dMRI signal simulations with no added noise (bar), with added SNR of 100 and no averaging (▽), and with SNR of 100 and 10 averages (⋆). Error bars are confidence intervals.

Table 1: Range of input parameters used in Sobol sensitivity study; parameters span range of experimentally observed values.

Parameter	Range			References
Myocyte Diameter	10	- 80	μm	[47, 52–57]
Myocyte Volume Fraction	0.70	- 0.95		[55, 58, 59]
Sarcolemma Membrane Permeability	10	- 100	$\mu m/s$	[47, 56, 60, 61]
Intracellular Diffusion Coefficient	0.5	- 2.5	$\mu m^2/ms$	[49, 58, 62, 63]
Extracellular Diffusion Coefficient	0.5	- 2.5	$\mu m^2/ms$	[49, 58, 62, 63]
Intracellular T_2 Relaxation Time	20	- 40	ms	[8, 58, 62–66]
Extracellular T_2 Relaxation Time	80	- 140	ms	[62–65]
Gradient Strength	10	- 80	mT/m	
Diffusion Time	10	- 750	ms	[22, 41, 67]

Table 2: Selected second-order indices for noise-free results. See supplementary information for all second-order results.

Fractional Anisotropy (FA)			
Diameter	&	Volume Fraction	0.08 ± 0.04
Diameter	&	Intracellular Diffusion	0.05 ± 0.04
Mean Diffusivity (MD)			
Volume Fraction	&	Extracellular Diffusion	0.05 ± 0.02
Radial Diffusivity (RD)			
Diameter	&	Volume Fraction	0.04 ± 0.03
Volume Fraction	&	Extracellular Diffusion	0.04 ± 0.02
Primary Eigenvalue (λ_1)			
Volume Fraction	&	Intracellular Diffusion	0.06 ± 0.02
Volume Fraction	&	Extracellular Diffusion	0.06 ± 0.02
Secondary Eigenvalue (λ_2)			
Diameter	&	Volume Fraction	0.04 ± 0.03
Volume Fraction	&	Extracellular Diffusion	0.04 ± 0.02
Tertiary Eigenvalue (λ_3)			
Diameter	&	Volume Fraction	0.04 ± 0.03
Volume Fraction	&	Extracellular Diffusion	0.04 ± 0.02